Archive of Applied Mechanics (2025) 95:36
https://doi.org/10.1007/s00419-024-02749-5

ORIGINAL

Kai He · Chang Peng

Iterative algorithm for the conformal mapping from the unit disk to domains with regular boundaries

Received: 19 August 2023 / Accepted: 23 December 2024 / Published online: 3 January 2025

Abstract Conformal mapping functions have significant applications in mechanics and other fields, and their computation methods have drawn considerable attention. We propose an iterative algorithm to compute the conformal mapping from the unit disk to physical domains with regular boundaries, defined by having only prime ends of the first kind. The mapping function is expanded into a Laurent series and use its truncated partial sum as an approximation. The Schwarz–Christoffel mapping formula provides the initial estimates for the series coefficients, which are then iteratively optimized. This algorithm efficiently handles complex domain shapes, such as winding orifices and slits, with high computational speed. Moreover, it offers valuable insights for designing algorithms to solve other types of conformal mapping problems and has practical significance in applications involving conformal mappings.

Keywords Conformal mapping function · Regular boundaries · Schwarz–Christoffel mapping formula · Laurent series

1 Introduction

Conformal mapping studies complex variable functions from a geometric perspective, transforming one region (canonical domain) into another (physical domain) through an analytic function. This property can map some irregular boundaries or boundaries difficult to express by mathematical formulas to regular or mature regional boundaries. Conformal mapping has been instrumental in addressing various important topics across fields such as digital image correlation techniques [1], the design of spatially varying orthotropic porous structures [2], the analysis of plastic zones around orifices [3], and the Steklov eigenvalue problem [4], among others [5–7]. For instance, Muskhelishvili utilized the conformal mapping from the interior of the unit circle to the exterior of an orifice to develop methods for solving stress distribution problems in infinite plates with arbitrary orifices [8]. This approach has been widely applied to analyze stress distributions in tunnel surrounding rock [9–11] and to calculate various crack intensity factors [12].

The Schwarz–Christoffel (SC) mapping formula has successfully solved many types of conformal mapping problems [13, 14]. However, these methods are predominantly applied to physical domains with polygonal boundaries. Although there are SC mapping formulas for curved boundaries, they require solving double integrals, which is computationally challenging [14]. For physical domains with curved boundaries, a common approach is to approximate the curved boundary with polygons that have a large number of vertices and then apply the SC mapping formula. This method, known as the polygon approximation algorithm, incurs significant computational cost.

K. He (✉) · C. Peng
School of Civil Engineering and Transportation, South China University of Technology, Guangzhou 510640, China
e-mail: kai.hee@foxmail.com

When the canonical domain is the unit disk and the physical domain is the exterior of a polygon, the conformal mapping function can be directly computed using the SC mapping formula [14]. However, the SC formula involves an integral whose analytical expression is often difficult to determine. In practice, even after obtaining an accurate mapping function via the SC formula, it is often expanded into a Laurent series for further applications [8]. For curved boundaries, early approaches relied on geometric construction, where approximate solutions were derived graphically, resulting in low accuracy. It is now established that conformal mapping functions can be expanded into Laurent series of a fixed form [8, 14]. By truncating the series, the mapping function can be approximated by solving for the partial sum. The image of the partial sum serves as an approximate representation of the boundary, and the difference between this image and the actual boundary is minimized to determine the coefficients.

Because the conformal mapping function is univalent, its coefficients must satisfy certain constraints [15, 16]. There are two main strategies for solving these coefficients: (1) directly optimizing the series coefficients using optimization algorithms, or (2) iteratively optimizing the coefficients. Hu et al. [15] and Wu et al. [16] adopted the first strategy to compute conformal mapping functions for some simple convex apertures. However, using optimization algorithms often leads to a complex algorithmic structure to enforce coefficient constraints, and the computational cost increases significantly as the number of terms in the partial sum grows. For complex boundary shapes, such as winding orifices, conformal mapping functions require the partial sum with many terms for accurate approximation, sometimes involving hundreds of terms. In such cases, optimization algorithms become impractical due to their computational cost. By contrast, iterative strategies significantly reduce computational complexity and are suitable. Huangfu et al. [17], Zhu et al. [18], and Nazem et al. [19] successfully applied iterative methods to compute conformal mapping functions for various simple closed curves, demonstrating their effectiveness in handling complex boundary shapes.

For certain complex boundary shapes, such as winding orifices or winding slits, existing methods often fail to achieve satisfactory results. Previously, we proposed an iterative algorithm to compute the conformal mapping function from the unit disk to a physical domain bounded by a simple closed curve [20]. However, this algorithm uses a Cartesian coordinate system to describe boundary shapes, making it unsuitable for non-convex boundaries. Similar limitations are also observed in other iterative algorithms. To address these issues and compute the conformal mapping function for arbitrary boundaries more effectively, we propose a new iterative algorithm, focusing on boundaries characterized by having only prime ends of the first kind. This algorithm employs arc length parametrization to represent boundary shapes, thereby eliminating the constraints imposed by coordinate systems. The SC mapping formula is used to estimate the initial values of the Laurent series coefficients, which are then iteratively optimized to reduce computational costs. This approach efficiently computes conformal mapping functions with thousands of series terms at high speed and can handle complex shapes, such as winding slits, which are critical for solving crack intensity factors [12].

2 Algorithm foundation and structure

2.1 Algorithm foundation

The Riemann mapping theorem states that for a simply connected region (physical domain) outside a simple closed curve on the real plane (z-plane), there exists a conformal mapping function that maps the unit disk (canonical domain) on the complex plane (ξ - plane) to the exterior of the curve, as shown in Fig. 1. A slit can be considered as an orifice with zero area, to which the Riemann mapping theorem still applies. The boundary Γ of the physical domain contains only prime ends of the first kind. This mapping can be expressed as:

$$z = \omega(\xi) \tag{1}$$

$$\Gamma = \omega(\partial\mathbb{D}), \mathbb{D}=\{\xi : |\xi| < 1\} \tag{2}$$

where the complex $z = x + i \cdot y$ represents the coordinates of the point on the z-plane, and the complex $\xi = \rho \cdot e^{i\theta}$ represents the coordinates of the point on the ξ - plane. For an arbitrary boundary, the mapping function typically lacks an exact expression in terms of finite elementary functions, or such an expression is challenging to determine. However, the mapping function can be expanded into Laurent series:

$$\omega(\xi)= \sum_{n=-1}^{+\infty} c_n \cdot \xi^n \tag{3}$$

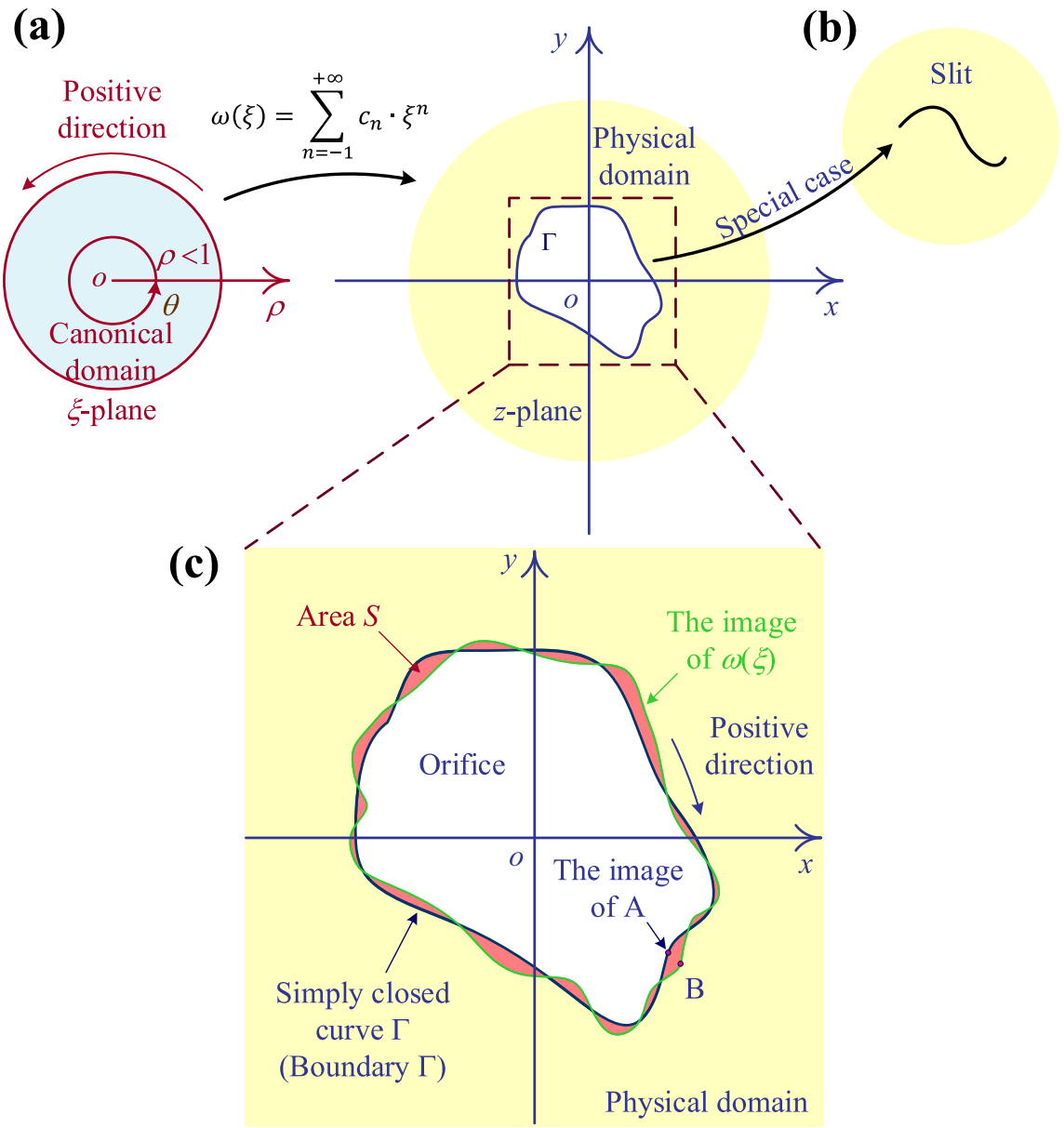

Fig. 1 **a** Conformal mapping from the canonical domain (the unit disk) to the physical domain (the exterior of a simple closed curve). **b** A slit can be regarded as a special case of an orifice, essentially representing an orifice with zero area. **c** The difference between the image of ω and the simple closed curve

where, in general, the coefficient c_n is a complex number. When the curve Γ is symmetric about the y axis, c_n is a real number. When the curve Γ is symmetric about the x axis, c_n is a pure imaginary number. It is vice versa: When the curve Γ is symmetric about the x axis, c_n is a real number. When the curve Γ is symmetric about the y axis, c_n is a pure imaginary number. And it is hold only if we normalize function ω as $\omega(0) = \infty$ and $\arg \frac{1}{\omega'(0)} = 0$.

In practical applications, the partial sum of the Laurent series (3) is used as an approximation of the conformal mapping function ω. The partial sum is:

$$\omega_N(\xi) = \sum_{n=-1}^{N} c_n \cdot \xi^n \tag{4}$$

The conformal mapping function ω_N maps the points on the ξ - plane to the figure on the z-plane, which is called the image of ω_N. The unit circle (excluding points inside or outside the circle) on ξ - plane is mapped to the curve Γ' on the z-plane. With the increase in the number of terms in the partial sum, the image of ω_N gradually approaches the physical domain, and the curves Γ' and Γ gradually coincide. In this process, the area S enclosed by curves Γ' and Γ gradually decreases (Fig. 1c). If there is a group of coefficients that can make the image of ω_N completely coincide with the physical domain, that is, the curves Γ' and Γ completely coincide, and then, the conformal mapping function ω_N at this time is accurate. However, for curve Γ with arbitrary shape, there is no such group of coefficients c_n more often. We hope to find such a group of coefficients c_n, so that the coincidence degree between the image of ω_N and the physical domain reaches the maximum or near the maximum, that is, the area S reaches zero or near zero.

Through the above analysis, we can easily find that the area S is only related to curves Γ' and Γ. In fact, there is a boundary correspondence principle [8], that is, if the conformal mapping function ω_N maps the unit circle to the curve Γ, the conformal mapping function ω_N maps the unit disk to the physical domain. After that, we will convert the conformal mapping function for solving the domain–domain to the mapping function for solving the curve–curve. At this time, take $\rho = 1$. When the partial sum ω_N is used to approximate the conformal mapping function, the coordinates of any M points on the curve Γ' are expressed in matrix $\mathbf{z}$ as:

$$z = \Xi \cdot c \tag{5}$$

where matrix $\boldsymbol{\theta}$ represents the phase angle of these points on ξ - plane. These matrices are:

$$\begin{cases} \mathbf{z} = [z_1, z_2, \cdots, z_M]^{\mathrm{T}} \\ \mathbf{c} = \left[c_{-1}, c_0, c_1, c_2, \cdots, c_N\right]^{\mathrm{T}} \\ \boldsymbol{\Xi} = \left[e^{ik\theta_j}\right],\ k \in \overline{-1, N},\ j \in \overline{1, M} \end{cases} \tag{6}$$

Assume ξ_{A} is any point A on the unit circle, and the image of point A is $z_{\mathrm{A}} = \omega_N(\xi_{\mathrm{A}})$. There is one and only one point B on the curve Γ. When the parameter N approaches infinity, the image of point A approaches point B infinitely. We refer to points with such a relationship as point A and B as a pair of corresponding points. We select M points on the unit circle and represent them with the set $\mathbf{A} = \{\mathrm{A}_1, \mathrm{A}_2, ..., \mathrm{A}_m, ..., \mathrm{A}_M\}$. Their coordinates are marked as $\boldsymbol{\xi}_{\mathrm{A}} = \exp(i \cdot \boldsymbol{\theta})$(Element-wise exponential operation), and the coordinates of their image are marked as $\mathbf{z}_{\mathrm{A}} = \omega_N\left(\boldsymbol{\xi}_{\mathrm{A}}\right)$. The matrix $\boldsymbol{\theta} = [\theta_1, \theta_2, \cdots, \theta_M]^{\mathrm{T}}$ represents the phase angle of these points on ξ - plane. The corresponding points of the points in set $\mathbf{A}$ are marked as set $\mathbf{B} = \{\mathrm{B}_1, \mathrm{B}_2, ..., \mathrm{B}_m, ..., \mathrm{B}_M\}$, and its coordinates are marked as $\mathbf{z}_{\mathrm{B}}$. The shape of curve Γ is described using function $z = f_\Gamma(s)$. The function $z = f_\Gamma(s)$ uses the arc length s to calculate the coordinates, whereby the coordinates of the point in set $\mathbf{B}$ can be determined:

$$\mathbf{z}_{\mathrm{B}} = f_\Gamma(\mathbf{s}_{\mathrm{B}}) \tag{7}$$

where the matrix $\mathbf{s}_{\mathrm{B}}$ is

$$\mathbf{s}_{\mathrm{B}} = \left[s_1^{\mathrm{B}}, s_2^{\mathrm{B}}, ..., s_m^{\mathrm{B}}, ..., s_M^{\mathrm{B}}\right]^{\mathrm{T}} \tag{8}$$

Similarly, we also use the arc length s to determine the coordinates of points on the curve Γ'. When using the arc length s, we need to determine the starting point of curve Γ' and make its corresponding point the starting point of curve Γ. Let the starting points of curves Γ' and Γ be points A_1 and B_1 in sets $\mathbf{A}$ and $\mathbf{B}$. Therefore, in Eq. (8), s_m^{B} represents the arc length from the point B_m to the starting point B_1 of the curve Γ.

When $2(N+2) < M$, using the least square method, we can calculate the coefficient $\mathbf{c}$ through the coordinate $\mathbf{z}_{\mathrm{A}}$ and Eq. (5) by

$$\mathbf{c} = \left(\boldsymbol{\Xi}^{\mathrm{T}} \cdot \boldsymbol{\Xi}\right)^{-1} \cdot \boldsymbol{\Xi}^{\mathrm{T}} \cdot \mathbf{z}_{\mathrm{A}} \tag{9}$$

We need to know $\mathbf{z}_{\mathrm{A}}$ and $\boldsymbol{\xi}_{\mathrm{A}}$ (or $\boldsymbol{\theta}$), meanwhile, to obtain the coefficient $\mathbf{c}$ through the above formula. We can specify a group of $\boldsymbol{\xi}_{\mathrm{A}}$ in advance and then find $\mathbf{z}_{\mathrm{A}}$. The coefficient $\mathbf{c}$ is different for different starting points. Assuming that D_1 and D_2 are two different starting points, and $\mathbf{c}_1$ and $\mathbf{c}_2$ are the coefficients determined by the starting points D_1 and D_2, respectively. The relationship between $\mathbf{c}_1$ and $\mathbf{c}_2$ is:

$$c_n^2 = c_n^1 \cdot \exp\left(i \cdot n \cdot \left[\theta_2^{\mathrm{D}} - \theta_1^{\mathrm{D}}\right]\right),\ n = -1, 0, 1, ..., N \tag{10}$$

When M is large and the distribution of corresponding points is relatively uniform, the arc length s of the points in set $\mathbf{A}$ can be approximated as:

$$s_m^{\mathrm{A}} \approx \begin{cases} 0,\ m = 1 \\ \sum_{k=2}^{m} \left| z_k^{\mathrm{A}} - z_{k-1}^{\mathrm{A}} \right|,\ m = 2, 3, ..., M \end{cases} \tag{11}$$

When the conformal mapping function ω_N is completely accurate, $s_m^{\mathrm{A}} = s_m^{\mathrm{B}}$ is established. When the function ω_N is an approximate solution, $s_m^{\mathrm{A}} \approx s_m^{\mathrm{B}}$ holds approximately. However, in the actual calculation process, due to the large difference between the length s_Γ of the curve Γ and the length s_ω of the curve Γ', the relationship $s_m^{\mathrm{A}} \approx s_m^{\mathrm{B}}$ is often not well satisfied. Especially when m takes a large value, it is easy to generate a large cumulative error when calculating the arc length using Eq. (11). Therefore, the arc length s_m^{B} and s_m^{A} are normalized using the lengths s_Γ and s_ω:

$$\eta_m^{\mathrm{A}} = \frac{s_m^{\mathrm{A}}}{s_\omega},\ \eta_m^{\mathrm{B}} = \frac{s_m^{\mathrm{B}}}{s_\Gamma} \tag{12}$$

where s_ω can be approximately calculated by:

$$s_\omega \approx \sum_{k=2}^{M} \left| z_k^{\mathrm{A}} - z_{k-1}^{\mathrm{A}} \right| + \left| z_1^{\mathrm{A}} - z_M^{\mathrm{A}} \right| \tag{13}$$

Use the function $\eta_m^{\mathrm{A}} = f_s\left(z_m^{\mathrm{A}}\right)$ to represent the calculation method of η_m^{A}. When function ω_N is an approximate solution, the ratio η_m^{A} and η_m^{B} can better satisfy $\eta_m^{\mathrm{A}} \approx \eta_m^{\mathrm{B}}$.

The SC mapping formula can map the unit disk to the exterior of a polygon on z-plane, as shown in Fig. 2. Its formula is

$$\omega_{\mathrm{SC}}(\xi) = \beta_1 \cdot \int_{\xi_0}^{\xi} \frac{1}{\xi^2} \cdot \prod_{k=1}^{K} \left(1 - \frac{\xi}{\xi_k}\right)^{1-\alpha_k} \mathrm{d}\xi + \beta_2 \tag{14}$$

where the coefficient β_1 is related to the size and rotation of the image of the function ω_{SC}, and the coefficient β_2 is related to the translation. z_k represents the coordinate of the polygon vertex. ξ_k represents the point on the unit circle corresponding to vertex z_k. α_k represents the exterior angle of vertex z_k divided by π. In the SC mapping formulas, the vertex z_k is a known quantity, but ξ_k is an unknown quantity. The Schwarz–Christoffel toolbox developed by Tobin A. Driscoll [13] solves for the unknown variables ξ_k, as well.

We select a polygon with a small number of vertices to approximate the curved boundary and then use the coefficients of the Laurent series obtained from the SC mapping formula as the initial values for the iteration. Naturally, the vertices of the polygon should be denser in regions with high curvature, and particularly at points where the curvature changes abruptly, a vertex should be placed. In regions with low curvature, the vertices can be more sparsely distributed. Specifically, for boundary sections with zero curvature, vertices may be omitted. Based on this, we propose the following strategy for vertex selection. The curvature κ_Γ of the curve Γ is

$$\kappa_\Gamma(s) = \left| f_\Gamma''(s) \right| \tag{15}$$

We divide the curve Γ into segments based on the corners, ensuring that the function κ_Γ remains continuous on each sub-curve. We then approximate the curve Γ with a polygonal representation consisting of K vertices, where L of these vertices correspond to the known corners of the curve Γ. Based on the above analysis, we allocate K_l polygon vertices to each sub-curve based on the following strategy:

We divide the curve Γ into segments based on the corners, ensuring that the function κ_Γ remains continuous on each sub-curve. We then approximate the curve Γ with a polygonal representation consisting of K vertices, L of which correspond to the known corners of the curve. Based on the above analysis, we allocate K_l polygon vertices to each sub-curve according to the following strategy:

$$K_l = \mathrm{round}\left(\frac{1}{K - L} \cdot \frac{\int_{s_{l-1}}^{s_l} \kappa_\Gamma(s) ds}{\int_0^{s_\Gamma} \kappa_\Gamma(s) ds} \right),\ l = 1, 2, ..., L \tag{16}$$

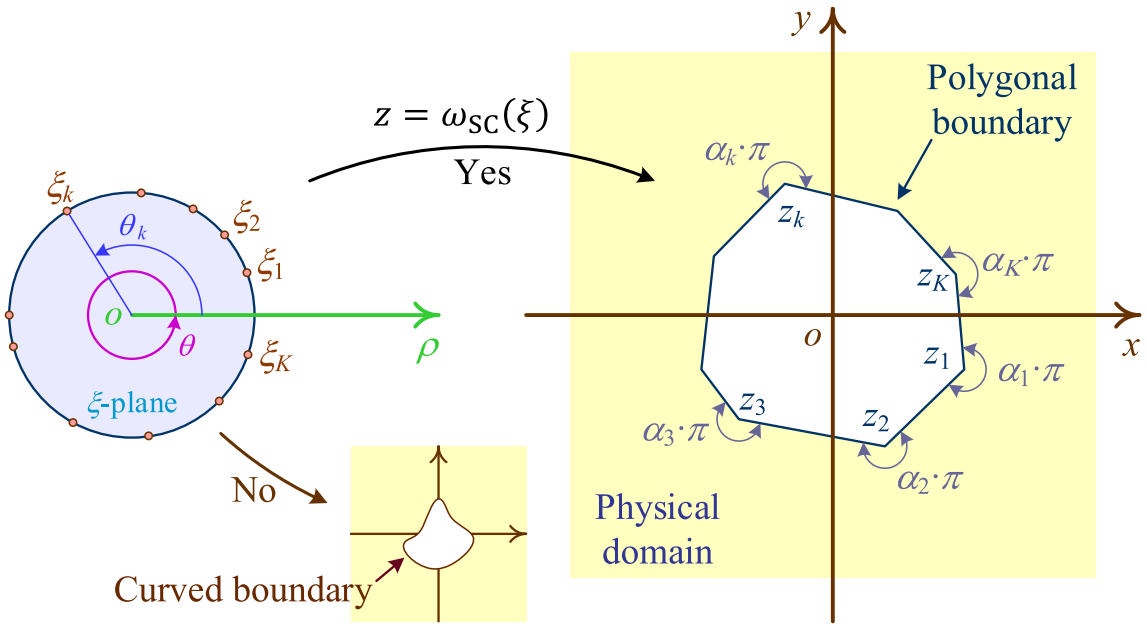

Fig. 2 Schematic diagram of Schwarz–Christoffel mapping formula

where subscript l indicates the l-th sub-curve. The function *round* represents the rounding operation. s_l represents arc length from the end point of the l-th sub-curve to the start point of Γ. The spacing of vertices on each sub-curve is:

where the subscript l indicates the l-th sub-curve. The function *round* represents the rounding operation. s_l denotes the arc length from the endpoint of the l-th sub-curve to the starting point of the curve Γ. The vertex spacing on each sub-curve is:

$$\Delta\kappa_l = \frac{1}{K_l} \cdot \int_{s_{l-1}}^{s_l} \kappa_\Gamma(s)ds,\ l = 1, 2, ..., L \tag{17}$$

We define several indicators to measure the accuracy of the conformal mapping function obtained by the algorithm. Naturally, the area S enclosed by curves Γ and Γ' can be regarded as the absolute error ε_Γ^a. When there are enough points in sets **A** and **B**, the absolute error ε_Γ^a can be expressed as Eq. (18). Furthermore, the ratio of the absolute error ε_Γ^a to the length s_Γ is called the relative error ε_Γ^r as Eq. (19).

$$\varepsilon_\Gamma^a = \left| \begin{bmatrix} z_M \\ \mathbf{z}_\mathrm{B} \end{bmatrix} - \begin{bmatrix} \mathbf{z}_\mathrm{B} \\ 0 \end{bmatrix} \right|^\mathrm{T} \cdot \left| \begin{bmatrix} \mathbf{z}_\mathrm{A} \\ 0 \end{bmatrix} - \begin{bmatrix} \mathbf{z}_\mathrm{B} \\ 0 \end{bmatrix} \right| \tag{18}$$

$$\varepsilon_\Gamma^r = \frac{\varepsilon_\Gamma^a}{s_\Gamma} \tag{19}$$

In addition, the difference between the curvature κ_Γ of curve Γ and the curvature κ_ω of curve Γ' is also extremely important. We can also define other error indicators as required.

2.2 Iterative algorithm

Select K vertices on the curve Γ to form a polygon and then solve the mapping function ω_{SC} by SC mapping formula. The starting point coordinate of the curve Γ' is determined to be $\omega_{SC}(1)$. Let the point closest to the point $\omega_{SC}(1)$ on the curve Γ be the starting point of the curve Γ. M points are uniformly selected on the curve Γ to form the set **B**. Use η_m^B to construct matrix $\boldsymbol{\eta}_0^\mathrm{B} = \left[\eta_1^\mathrm{B}, \eta_2^\mathrm{B}, ...\eta_m^\mathrm{B}, ..., \eta_M^\mathrm{B}\right]^\mathrm{T}$ as

$$\boldsymbol{\eta}_0^\mathrm{B} = \frac{1}{M} \cdot [0, 1, ..., M-1]^\mathrm{T} \tag{20}$$

The subscript of the symbol $\boldsymbol{\eta}_0^{\mathrm{B}}$ indicates the number of iterations. 0 indicates the initial value, and other symbols are similar. The coordinates $\mathbf{z}_0^{\mathrm{B}}$ of the points in set $\mathbf{B}$ are

$$\mathbf{z}_0^{\mathrm{B}} = f_\Gamma\left(s_\Gamma \cdot \boldsymbol{\eta}_0^{\mathrm{B}}\right) \tag{21}$$

At this time, there is $\mathbf{z}_0^{\mathrm{A}} \approx \mathbf{z}_0^{\mathrm{B}}$, and $\boldsymbol{\xi}_{\mathrm{A}}$ can be determined by the inverse function of ω_{SC}:

$$\boldsymbol{\xi}_{\mathrm{A}} \approx \omega_{\mathrm{SC}}^{-1}\left(\mathbf{z}_0^{\mathrm{B}}\right) \tag{22}$$

$\boldsymbol{\xi}_{\mathrm{A}}$ does not change during iteration. And then matrix $\boldsymbol{\Xi}$ can be computed using Eq. (6). The coefficient $\mathbf{c}$ can be calculated by iterating according to the following process:

$$\mathbf{z}_{gen}^{\mathrm{B}} = f_\Gamma\left(s_\Gamma \cdot \boldsymbol{\eta}_{gen}^{\mathrm{B}}\right) \tag{23}$$

$$\mathbf{c}_{gen} = \left(\boldsymbol{\Xi}^{\mathrm{T}} \cdot \boldsymbol{\Xi}\right)^{-1} \cdot \boldsymbol{\Xi}^{\mathrm{T}} \cdot \mathbf{z}_{gen}^{\mathrm{B}} \tag{24}$$

$$\mathbf{z}_{gen}^{\mathrm{A}} = \boldsymbol{\Xi} \cdot \mathbf{c}_{gen} \tag{25}$$

$$\boldsymbol{\eta}_{gen}^{\mathrm{A}} = f_s\left(\mathbf{z}_{gen}^{\mathrm{A}}\right) \tag{26}$$

$$\boldsymbol{\eta}_{gen+1}^{\mathrm{B}} = \lambda \cdot \boldsymbol{\eta}_{gen}^{\mathrm{A}} + (1-\lambda) \cdot \boldsymbol{\eta}_{gen}^{\mathrm{B}} \tag{27}$$

where, $0 < \lambda \leq 1$, reflect the speed of $\boldsymbol{\eta}_{gen}^{\mathrm{B}}$ update. The above iterative process can be summarized as:

$$\boldsymbol{\eta}_{gen+1}^{\mathrm{B}} = \lambda \cdot f_s\left(\boldsymbol{\Lambda} \cdot f_\Gamma\left(s_\Gamma \cdot \boldsymbol{\eta}_{gen}^{\mathrm{B}}\right)\right) + (1-\lambda) \cdot \boldsymbol{\eta}_{gen}^{\mathrm{B}} \tag{28}$$

where the matrix $\boldsymbol{\Lambda} = \boldsymbol{\Xi} \cdot \left(\boldsymbol{\Xi}^{\mathrm{T}} \cdot \boldsymbol{\Xi}\right)^{-1} \cdot \boldsymbol{\Xi}^{\mathrm{T}}$ does not change during iteration. In the iterative process of the algorithm, we define three convergence conditions: (a) the number of iterations, *gen*, reaches the maximum value; (b) the error reaches the threshold; and (c) the rate of change of the error is below a predetermined threshold. Other convergence conditions can also be defined.

3 Results

To demonstrate the performance of our proposed algorithm, we construct a winding orifice Γ_1 and a winding slit Γ_2. The shapes and analytical expressions are shown in Fig. 3a and b, respectively. We select 30 vertices to approximate the curves as polygonal shapes (Fig. 3a and b). Then, the SC mapping formula is applied to estimate the initial values of the Laurent series coefficients. In Fig. 3a and b, some key points are highlighted, including the starting point, the point with the largest error, and the point where the curvature changes abruptly (i.e., the cusp of the curve). We set the parameter N to 200. When the algorithm converges, as shown in Fig. 3c and d, the image of the conformal mapping function is displayed, demonstrating the effectiveness of the algorithm.

Figures 4 and 5 illustrate various details of the algorithm. Figure 4a shows the typical variation in relative error with respect to the number of iterations. The relative error gradually decreases until it stabilizes. Figure 4b demonstrates how the relative error changes as the number of the partial sum terms N increases. As N grows, the relative error decreases rapidly. Figure 5a and b depicts the distribution of the relative error along curves Γ_1 and Γ_2. The largest error occurs at the part of the curve where it bends inward toward the orifice. At the corners of curves, the error increases significantly. Figure 5c and d shows the curvature distribution along curves. The curvature of the conformal mapping function obtained by our algorithm closely matches that of the original curves. The solution obtained reasonably reflects the curvature of the curve.

We compared the polygon approximation algorithm based on the SC mapping formula, and the iterative algorithm presented in this paper. Figure 5 illustrates the details of these algorithms. Using strategies (16) and (17), a large number of vertices are distributed along the curved sections of the curves, forming a polygonal approximation. The SC mapping formula is then used to solve the conformal mapping function for this polygon and expand it into a Laurent series. Figure 4c shows that, with a fixed number of vertices, the error of the polygon approximation algorithm gradually converges to a certain value as the parameter N increases. Figure 5b indicates that, once the polygon approximation algorithm converges (i.e., the error does not change significantly with further increase in N), the error initially decreases rapidly with the increase in the number of vertices,

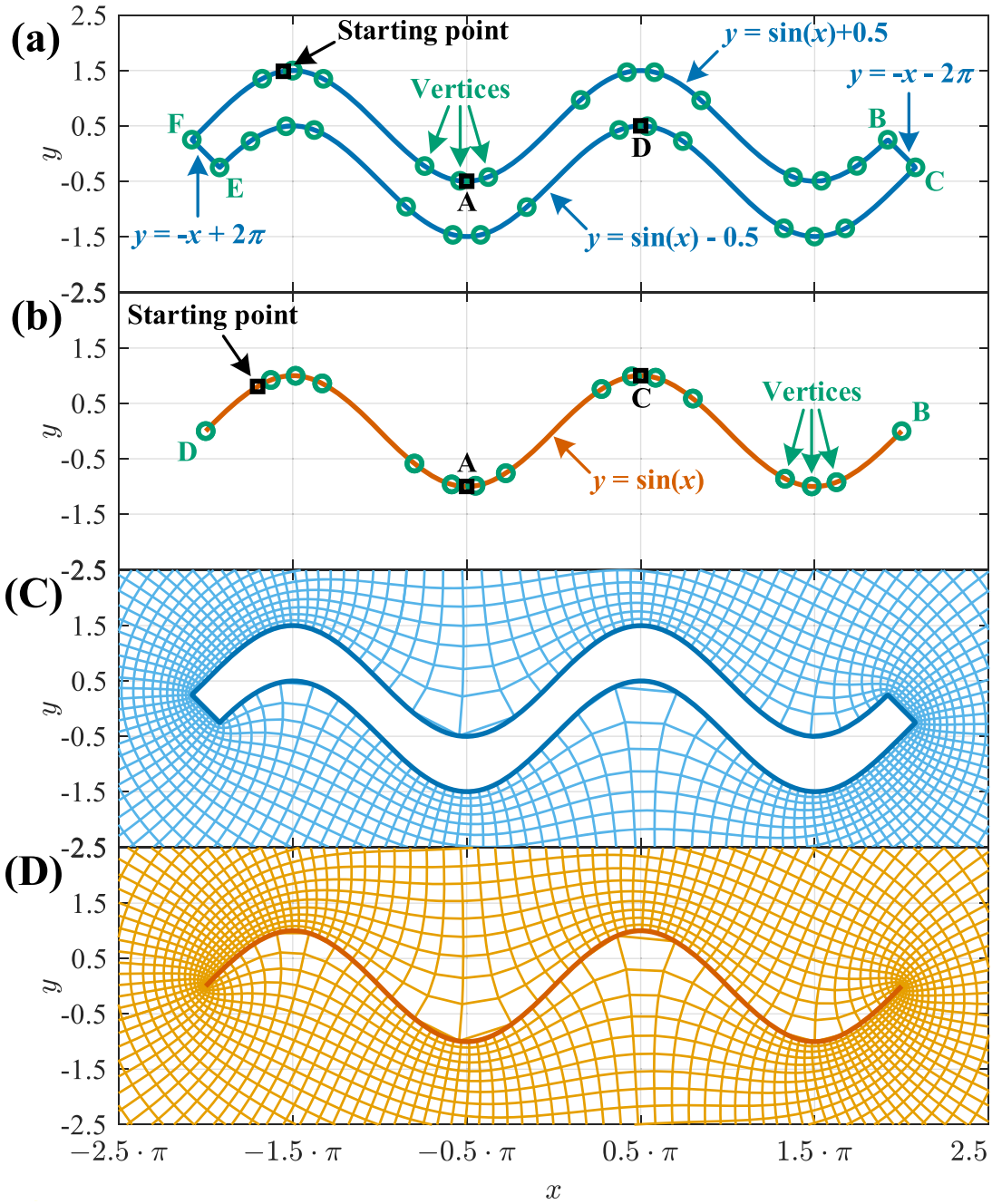

Fig. 3 Shapes and analytical expressions of curves **a** Γ_1 and **b** Γ_2. The images of conformal mapping function with curves **c** Γ_1 and **d** Γ_2

before leveling off. This phenomenon may be attributed to the limitations of finite precision in computing systems, where floating-point precision restricts further improvement in the algorithm's error. Additionally, when the number of vertices is large, the solution time for the SC mapping formula increases, taking several minutes. In contrast, the convergence time of the algorithm proposed in this paper is only a few tens of seconds. In conclusion, the polygon approximation algorithm, when increasing the number of vertices and the partial sum without restrictions, does not yield a conformal mapping function with significantly higher accuracy. The relative error, when the solution is optimized, stabilizes at around 10^{-3} (see Fig. 4c and d). On the other hand,

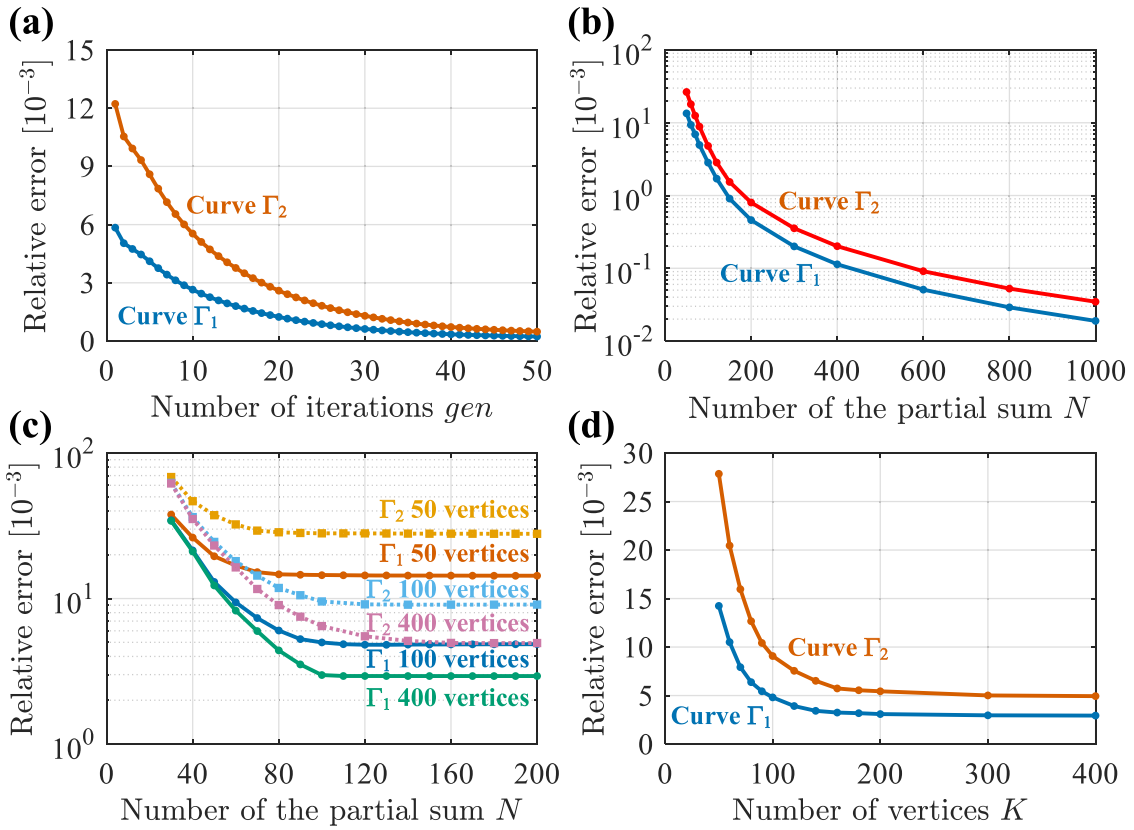

Fig. 4 **a** Variation of relative error with the number of iterations. **b** Variation of relative error with increasing partial sum terms N after the algorithm converges. **c** Relative error as a function of the number of partial sum terms N for different numbers of vertices in the polygon approximation algorithm. **d** Relative error as a function of the number of vertices after the polygon approximation algorithm converges

the accuracy of the algorithm proposed in this paper continues to improve with increasing the number of the partial sum, rapidly reaching a relative error as low as 10^{-5} (see Fig. 4b).

It is important to note that the discussion of the polygon approximation method here is not exhaustive. The performance of the polygon approximation method depends heavily on the selection of vertices, and different vertex selection strategies can lead to varying results. By tailoring the vertex selection to specific application requirements, it is possible to design more effective strategies to enhance the accuracy of the polygon approximation method.

4 Discussion and conclusion

This paper proposes an iterative algorithm for solving the conformal mapping function from the unit disk to the physical domains with regular boundaries. However, we have not provided a general theoretical proof of the algorithm's convergence. In practice, the algorithm we designed demonstrates good convergence and high accuracy in most cases. Through tests on boundaries of different shapes, we found that the algorithm could be sensitive to certain parameter combinations, resulting in reduced accuracy. Nevertheless, slight adjustments to the parameters within a small range can significantly improve accuracy. Additionally, for extreme cases, such as a C-shaped boundary with a narrow opening, the algorithm may fail to converge. Despite these limitations, the algorithm effectively solves conformal mapping functions for most complex shapes, underscoring its significance in practical applications of conformal mapping.

To facilitate research and applications, we have developed a MATLAB toolbox based on the algorithm proposed in this paper (https://github.com/e-2718/OpenConMap). The toolbox provides basic usage instructions, additional examples, and demonstrations of simple applications of conformal mapping functions. Readers interested in this topic are encouraged to download and use it.

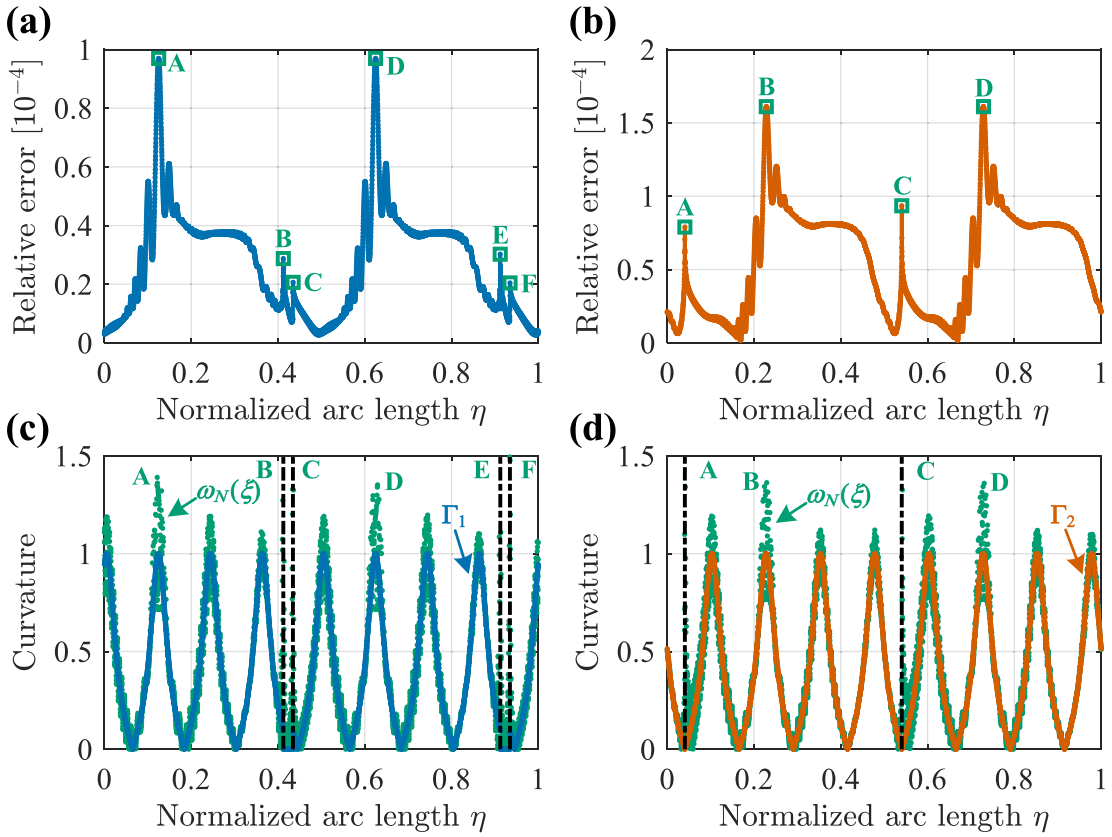

Fig. 5 The relative error distribution along the curves **c** Γ_1 and **d** Γ_2, and the curvature distribution along the curves **e** Γ_1 and **f** Γ_2

Acknowledgements We sincerely thank the reviewers and editors for their valuable time and effort during the review process of this manuscript. Their insightful and constructive comments helped us identify areas for improvement and further refine our research.

Author contributions Kai He did conceptualization, formal analysis, investigation, methodology, project administration, resources, software, supervision, validation, visualization, writing—original draft, and writing—review & editing. Chang Peng done data curation, formal analysis, funding acquisition, resources, software, validation, and writing—original draft.

Declarations

Conflict of interest The corresponding author states that there is no conflict of interest.

References

1. Ye, J., Ji, H., Zhang, X.: Digital image correlation method based on quasi-conformal mapping for large deformation measurement. Opt. Lasers Eng. **153**, 106985 (2022). https://doi.org/10.1016/j.optlaseng.2022.106985
2. Li, S., Zhu, Y., Guo, X.: Optimisation of spatially varying orthotropic porous structures based on conformal mapping. Comput. Method. Appl. Mech. Eng. **391**, 114589 (2022). https://doi.org/10.1016/j.cma.2022.114589
3. Ma, Y., Lu, A., Cai, H., Zeng, X.: An analytical method for determining the plastic regions around two circular holes in an infinite medium. Appl. Math. Model. **89**, 636–653 (2021). https://doi.org/10.1016/j.apm.2020.07.033
4. Alhejaili, W., Kao, C.-Y.: Numerical studies of the Steklov eigenvalue problem via conformal mappings. Appl. Math. Comput. **347**, 785–802 (2019). https://doi.org/10.1016/j.amc.2018.11.048
5. Abdelmoula, R., Semani, K., Li, J.: Analysis of cracks originating at the boundary of a circular hole in an infinite plate by using a new conformal mapping approach. Appl. Math. Comput. **188**, 1891–1896 (2007). https://doi.org/10.1016/j.amc.2006.11.052
6. Alshaya, A., Rowlands, R.: Experimental stress analysis of a notched finite composite tensile plate. Compos. Sci. Technol. **144**, 89–99 (2017). https://doi.org/10.1016/j.compscitech.2017.03.007

7. Liu, Y., Fu, J., Sun, F., He, S.: Magnifying lens designed by optical conformal mapping. Opt. Express **28**, 36892–36901 (2020). https://doi.org/10.1364/OE.412936
8. Muskhelishvili, N.I.: Some basic problems of the mathematical heory of elasticity. P. Noordhoff Ltd, Cambridge (1953)
9. Exadaktylos, G.E., Liolios, P.A., Stavropoulou, M.C.: A semi-analytical elastic stress–displacement solution for notched circular openings in rocks. Int. J. Solids Struct. **40**, 1165–1187 (2003). https://doi.org/10.1016/S0020-7683(02)00646-7
10. Tan, L., Ren, T., Dou, L., Yang, X., Qiao, M., Peng, H.: Analytical stress solution and mechanical properties for rock mass containing a hole with complex shape. Theor. Appl. Fract. Mech. **114**, 103002 (2021). https://doi.org/10.1016/j.tafmec.2021.103002
11. Zhao, G., Yang, S.: Analytical solutions for rock stress around square tunnels using complex variable theory. Int. J. Rock Mech. Min. Sci. **80**, 302–307 (2015). https://doi.org/10.1016/j.ijrmms.2015.09.018
12. Li, Y., Zheng, K.: Stress intensity factor analysis of kinked and hole crack in an infinite plate using numerical conformal mapping. Theor. Appl. Fract. Mech. **114**, 103022 (2021). https://doi.org/10.1016/j.tafmec.2021.103022
13. Driscoll, T.A.: Algorithm 756: a MATLAB toolbox for Schwarz-Christoffel mapping. ACM Trans. Math. Software **22**, 168–186 (1996). https://doi.org/10.1145/229473.229475
14. Driscoll, T.A., Trefethen, L.N.: Schwarz-Christoffel mapping, pp. 10011–14211. Cambridge University Press, New York (2002)
15. Hu, B., Li, C., Wei, X., Zhou, X., Gong, C., Wang, D.: Elastic stress solution for complex cross section of roadways based on genetic optimization and sequential quadratic programming algorithm. Chin. J. Rock Mech. Eng. **36**, 13 (2017). https://doi.org/10.13722/j.cnki.jrme.2016.0371
16. Wu, S., Li, K., Wu, S., Wang, H., Qin, Q., Li, M., He, F.: Analysis of geometric parameters of straight wall three-centered arch and stress of surrounding rock based on conformal mapping. Rock Soil Mech. **41**, 11 (2020). https://doi.org/10.16285/j.rsm.2020.0195
17. Huangfu, P.P., Wu, F.Q., Guo, S.F., Xiong, Z.: A new method for calculating mapping function of external area of cavern with arbitrary shape based on searching points on boundary. Rock Soil Mech. **32**(5), 1418–1424 (2011)
18. Zhu, J., Yang, J., Shi, G., Wang, J., Cai, J.: Calculating method for conformal mapping from exterior of unit circle to exterior of cavern with arbitrary excavation cross-section. Rock Soil Mech. **35**, 9 (2014). https://doi.org/10.16285/j.rsm.2014.01.025
19. Nazem, A., Hossaini, M.-F., Rahami, H., Bolghonabadi, R.: Optimization of conformal mapping functions used in developing closed-form solutions for underground structures with conventional cross sections. Int. J. Min. Geo Eng. **49**, 10 (2015). https://doi.org/10.22059/ijmge.2015.54633
20. He, K., Chang, J., Pang, D., Sun, B., Yin, Z., Li, D.: Iterative algorithm for the conformal mapping function from the exterior of a roadway to the interior of a unit circle. Arch. Appl. Mech. **92**, 971–991 (2022). https://doi.org/10.1007/s00419-021-02087-w